

HandNeRF: Learning to Reconstruct Hand-Object Interaction Scene from a Single RGB Image

Hongsuk Choi¹, Nikhil Chavan-Dafle¹, Jiacheng Yuan¹, Volkan Isler¹, and Hyunsoo Park¹

Abstract—This paper presents a method to learn hand-object interaction prior for reconstructing a 3D hand-object scene from a single RGB image. The inference as well as training-data generation for 3D hand-object scene reconstruction is challenging due to the depth ambiguity of a single image and occlusions by the hand and object. We turn this challenge into an opportunity by utilizing the hand shape to constrain the possible relative configuration of the hand and object geometry. We design a generalizable implicit function, HandNeRF, that explicitly encodes the correlation of the 3D hand shape features and 2D object features to predict the hand and object scene geometry. With experiments on real-world datasets, we show that HandNeRF is able to reconstruct hand-object scenes of novel grasp configurations more accurately than comparable methods. Moreover, we demonstrate that object reconstruction from HandNeRF ensures more accurate execution of a downstream task, such as grasping for robotic hand-over.

I. INTRODUCTION

The understanding of 3D hand-object interactions, i.e., semantic reconstruction of the hand and object geometry, is a key to applications such as human-to-robot object handover, and augmented and virtual reality. Despite significant interest in the recent years, this task remains highly challenging. Most of the current methods are primarily based on template-based approaches, where a known 3D CAD model of a hand and an object is assumed and the major focus is predicting the transformation that fits the known 3D CAD model to input observation [37], [12], [19].

Even under these assumptions, the hand and object reconstruction from a single RGB image are both difficult tasks due to depth ambiguity and mutual occlusions. In recent years, the 3D hand reconstruction has seen a significant advance [11], [26], [33] owing to large-scale hand datasets [46], [24], [2], [45]. In contrast, the progress in reconstruction of an hand-held object from a single RGB image is relatively limited due to lack of data. The topology of objects can infinitely vary across categories and instances. Generating a 3D CAD model of every object and labeling 6D poses in hand-object interaction scenes are labor-intensive and challenging, whereas 3D hand annotation is automated with reliable quality [27], [45] recently. Sparsity of views in a real-world data collection setting makes the labeling ambiguous, and inaccuracy of 6D pose annotation due to hand occlusions requires manual initialization and post-processing [35], [2].

In this regard, we present a new method that estimates a semantic neural radiance field of a hand-object interaction scene from a single RGB image. Our method, named HandNeRF, does not require an object template and predicts the

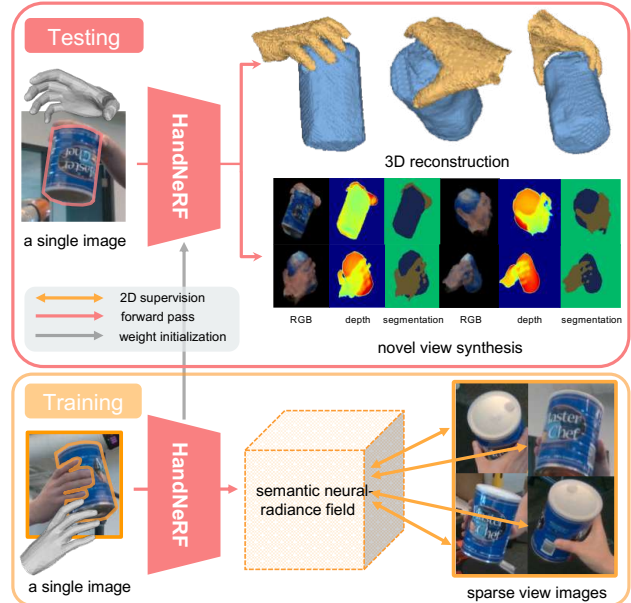


Fig. 1: Given a single RGB image of a hand-object interaction scene, HandNeRF predicts the hand and object’s density, color, and semantics, which can be converted to reconstruction of 3D hand and object meshes and rendered to novel view images (RGB, depth, and semantic segmentation). HandNeRF learns the correlation between hand and object geometry from different types of hand-object interactions, supervised by sparse view images. HandNeRF is tested on a novel scene with unseen hand-object interaction.

hand and object’s density (occupancy), color, and semantics, which are validated by synthesizing sparse view images during training. The key technical contribution of HandNeRF is that it alleviates the ill-posed 2D to 3D reconstruction problem by utilizing the hand shape to constrain the possible relative configuration of hand and object geometry. In particular, HandNeRF explicitly learns the correlation between hand and object geometry using the estimated 3D hand mesh and 2D object segmentation, which differs from relevant works [42], [41], [3]. Fig. 1 illustrates HandNeRF that is learned from sparse view RGB images, resulting in high-quality 3D reconstruction and rendering of images from a single RGB input.

HandNeRF is trained on multiple hand-object interaction scenes, where each scene has synchronized sparse view RGB images, 3D hand mesh annotation, and semantic segmentation, to learn the correlation between hand and object geometry. In inference time, a single RGB image with a novel grasp configuration is given. The object used in training and testing

¹Samsung AI Center, New York

can be the same following previous works [5], [41], but the grasp configuration is kept significantly different. Note that we do not use depth information in the whole process, which is much more unconstrained setting for both training and testing.

We evaluate HandNeRF on multiple realworld datasets including DexYCB [2] and HO-3D v3 [10] in terms of novel view synthesis and 3D reconstruction. We compare HandNeRF with the relevant sparse view-specific NeRF baselines [42], [41], [3] which we adapt to the task of reconstructing hand-object interaction in the same setting as HandNeRF. By learning the hand-object interaction prior with the explicit modeling of hand and object correlation, HandNeRF outperforms the baselines in generalization to both novel hand grasp and novel object shape. Furthermore, we quantitatively and qualitatively demonstrate that HandNeRF enables more accurate execution of a downstream task, such as grasping for robotic hand-over.

II. RELATED WORK

Our work, HandNeRF, lies at the intersection of understanding 3D hand-object interaction and implicit neural representations. In this section, we first review the current approaches for 3D hand-object interaction reconstruction from a single RGB camera. Then, we discuss recent methods for sparse view-specific implicit neural representations, relevant to our work.

3D reconstruction of hand-object interaction. The study on the understanding of 3D hand-object interactions [31], [35], [13], [1] refers to semantic reconstruction of the hand and object geometry. In the context of this task, the existing methods for hand and object reconstruction are primarily based on template-based approaches, where the template indicates a known 3D CAD model of a hand and an object. The 3D hand reconstruction focuses on predicting mesh parameters, such as MANO [32], and has seen a significant advance owing to large-scale datasets [46], [2], [45] and success of deep learning-based approaches [6], [33], [23]. Whereas, the 3D object reconstruction is approached as 6D pose estimation [37], [12], [19], which predicts the transformation that fits the known 3D CAD model to input observation.

The template-based approach for object reconstruction has two main limitations regarding collection of training data in the real world. First, it is costly and labor-intensive to obtain every object’s 3D CAD model, requiring 3D laser scanning or a dense multi-view camera setup. Second, labeling 6D object poses in hand-object scenes is challenging due to hand occlusions and becomes more ambiguous if the captured views are not dense enough. In contrast, for training HandNeRF we require only a few sparse RGB views of hand-object interaction scenes and hand-pose annotations which can be automated [27], [45].

Recently, [13], [16], [41] proposed methods that reconstruct a hand-held object without a known template. The work of Hasson et al. [13] jointly estimated the MANO hand parameters and genus-0 object mesh by leveraging

AtlasNet [8]. Karunratanakul et al. [16] characterized the surface of the hand and object with a signed distance field. Ye et al. [41] conditioned object reconstruction on the hand articulation and also predicted a signed distance field of an object. While the three methods are template-free in inference time, they require 3D object meshes for training, making them to share the fundamental data collection problem as the template-based methods.

Implicit neural representation from sparse view images.

The sparse view-specific NeRF (Neural Radiance Field) representations have gathered attention in object and scene-level reconstruction [42], [39], [15], [25] and 3D human body reconstruction [40], [28], [17], [3]. Without the 3D annotation that requires a demanding labeling process, they reconstruct a plausible 3D scene when optimized over a single scene only with sparse views. These methods address the limitations of previous multi-view reconstruction approaches such as vanilla NeRF [22] and SfM (Structure from Motion) which require a highly dense capture setup, over 100 views, and fails when given sparse views as addressed in the work of Leroy et al. [18]. These representations are also explored for generalization by learning object appearance and geometry priors from multiple scenes. When tested on novel scenes with unseen 6D object poses or unseen objects, a partial 3D reconstruction is achieved, although with blurry textures and noisy geometry. This limited performance is inevitable due to sparsity of the given input views, but the practical applications of these methods is significant. Nevertheless, scenes with a single view are less studied and hand-held objects are not explored in the sparse view-specific NeRF literature, despite their importance.

Our work is most relevant to the work of Choi et al. [3], MonoNHR, which reconstructs a neural radiance field of a clothed human body from a single RGB image without ground truth 3D scans of clothed human. MonoNHR conditions the clothed human’s texture and geometry estimation on SMPL [20] body mesh and proposes a novel geometry-dedicated feature. In this paper, we apply MonoNHR to hand-object interaction scenes, where a body mesh and clothes correspond to a hand mesh and an object respectively, and compare with our HandNeRF.

III. METHOD

The key motivation for HandNeRF is to tackle the challenges of 3D reconstruction from a 2D RGB image such as depth uncertainties and partial observation, especially given no 3D ground truth of objects. HandNeRF achieves this by learning hand-object interaction feature that correlates the hand and object geometry, given a 3D hand shape and 2D object segmentation. In essence, this feature encodes prior knowledge of hand geometry that imposes constraints on the local and global relative configurations between the hand and object geometry.

A. Modeling Hand-object Interaction

Consider a point on a 3D object, $\mathbf{x}_o \in \mathbb{R}^3$ where its occupancy or density is $\sigma \in [0, 1]$, i.e., one is occupied,

and zero otherwise. The problem of 3D reconstruction of the object can be cast as learning a function that predicts the density given the location and associated 3D feature \mathbf{f}_o :

$$f(\mathbf{x}_o, \mathbf{f}_o) = \sigma, \quad (1)$$

where f is an implicit function of which zero-level set defines the surface of the object. Despite the success of representing objects [42] and humans [34], Equation (1) has a limited capability to express complex scenes such as hand-object interaction scenes.

We extend Equation (1) by incorporating the interactions between the object and hand. Consider a 3D hand mesh $\mathcal{M} = \{\mathbf{m}_i\}_i$ that is made of a set of faces where \mathbf{m}_i is the i^{th} face of the mesh. Each face in the mesh is associated with a 3D feature \mathbf{f}_h . We marginalize the density of the object over the density predicted by the hand mesh:

$$f(\mathbf{x}_o, \mathbf{f}_o) = \sum_{\mathbf{x}_h \in \mathcal{M}} f(\mathbf{x}_o, \mathbf{f}_o | \mathbf{x}_h, \mathbf{f}_h) f(\mathbf{x}_h, \mathbf{f}_h), \quad (2)$$

where \mathbf{x}_h is the centroid of the vertices of the face \mathbf{m}_i , $f(\mathbf{x}_o, \mathbf{f}_o | \mathbf{x}_h, \mathbf{f}_h)$ is the conditional density given the hand pose and its feature. $f(\mathbf{x}_h, \mathbf{f}_h) = \{0, 1\}$ is the hand occupancy provided by 3D hand mesh estimation.

Learning $f(\mathbf{x}_o, \mathbf{f}_o | \mathbf{x}_h, \mathbf{f}_h)$ is challenging due to the quadratic complexity of pairwise relationship, i.e., all possible pairs of hand and object points $(\mathbf{x}_h, \mathbf{x}_o)$ need to be considered. Instead, we propose to learn an interaction feature \mathcal{F} , a correlation between \mathbf{f}_o and \mathbf{f}_h through a series of 3D convolutions:

$$\mathcal{F} = \phi_n \circ \dots \circ \phi_1 \circ \mathcal{V}, \quad (3)$$

where $\mathcal{F} \in \mathbb{R}^{w \times h \times d \times c}$ is the volume of the interaction features with w width, h height, d depth, c feature dimension, and ϕ_1, \dots, ϕ_n are the 3D convolutional filters. The interaction feature $\mathcal{F}|_{\mathbf{x}_o}$ evaluated at an object point \mathbf{x}_o is expected to encode how a point in hand contributed to predicting the occupancy of the point \mathbf{x}_o in the object. The input to the 3D CNN is $\mathcal{V} \in \mathbb{R}^{w \times h \times d \times c'}$, which is the feature volume with the c' feature dimension that includes both hand and object features:

$$\mathcal{V}_{\mathbf{x}} = \begin{cases} \mathbf{f}_h & \text{if } \mathbf{x} \in \mathcal{M} \\ \mathbf{f}_o & \text{if } \Pi \mathbf{x} \in \mathcal{O} \\ \mathbf{0} & \text{otherwise} \end{cases}, \quad (4)$$

where $\mathcal{V}_{\mathbf{x}}$ is the feature at \mathbf{x} , $\Pi \mathbf{x}$ is the camera projection of \mathbf{x} to the input image, and \mathcal{O} is the 2D input object mask.

With the interaction feature, we extend Equation (1) to include the color, $\mathbf{c} \in \mathbb{R}^3$, and semantic label $\mathbf{l} \in [0, 1]^L$ where $L = 3$ is the number of semantic classes (e.g., hand, object, and background):

$$f(\mathbf{x}_o, \mathbf{d}, \mathbf{f}_{2D}, \mathcal{F}|_{\mathbf{x}_o}) = (\sigma, \mathbf{c}, \mathbf{l}), \quad (5)$$

where \mathbf{d} is the rendering viewing direction, and \mathbf{f}_{2D} is the pixel-aligned image feature of \mathbf{x}_o .

Fig. 2 illustrates the impact of the 3D hand-object interaction features given an input image where we compare our method with MonoNHR [3] that does not explicitly

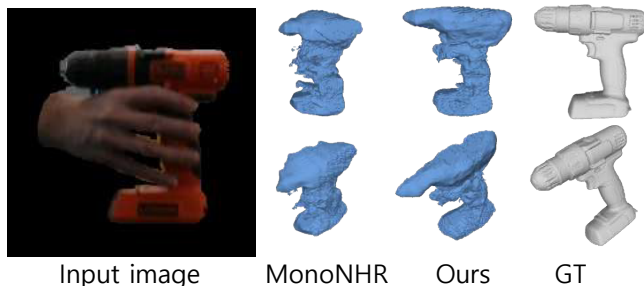


Fig. 2: Both our method and MonoNHR encode image features in a volumetric 3D space with a 3D CNN. However, different from MonoNHR, our method explicitly learn the hand-object interaction feature and produces better overall geometry of an object from an input image.

encode hand-object interactions. Our explicit representation is learned by a series of 3D convolutions that establish long-distance interaction, which allows successfully reconstructing the 3D geometry of the object while MonoNHR suffers from the incomplete reconstruction.

Given the prediction of the volume density, color radiance, and semantic label, we render each pixel with its label by integrating the density field:

$$C(\mathbf{p}) = \sum_{j=1}^N T_j (1 - \exp(-\sigma(\mathbf{x}_j) \delta_j)) \mathbf{c}(\mathbf{x}_j),$$

$$L(\mathbf{p}) = \sum_{j=1}^N T_j (1 - \exp(-\sigma(\mathbf{x}_j) \delta_j)) \mathbf{l}(\mathbf{x}_j),$$

$$\text{where } T_j = \exp\left(-\sum_{k=1}^{j-1} \sigma(\mathbf{x}_k) \delta_k\right),$$

where $C(\mathbf{p})$ is the expected RGB value at the pixel $\mathbf{p} \in \mathbb{R}^2$ where \mathbf{x}_j is the j^{th} sampled point along the 3D ray of \mathbf{p} from the target view, i.e., the inverse projection of \mathbf{p} . $\delta_i = \|\mathbf{x}_{i+1} - \mathbf{x}_i\|_2$ is the distance between adjacent sampled points. $L(\mathbf{p})$ is the expected semantic value of \mathbf{p} . Please refer to Semantic-NeRF [44] for more technical detail of rendering.

B. Implementation of HandNeRF

We learn the representation of the hand-object interaction by minimizing the following loss:

$$\mathcal{L} = \sum_{\mathbf{p} \in \mathcal{R}} \left(\left\| \hat{C}(\mathbf{p}) - C(\mathbf{p}) \right\|_2^2 - \sum_{i=1}^L L_i(\mathbf{p}) \log(\hat{L}_i(\mathbf{p})) \right)$$

where \mathcal{R} is a set of pixels in multiview images, $\hat{C}(\mathbf{p})$ and $C(\mathbf{p})$ are the predicted and ground truth color of pixel \mathbf{p} , respectively, and $\hat{L}_i(\mathbf{p})$ and $L_i(\mathbf{p})$ are the predicted and ground truth semantic label at pixel \mathbf{p} .

We design a novel network called *HandNeRF* that predicts a semantic neural radiance field from a single RGB image, as shown in Fig. 3. It is composed of ResNet-18 [14] for

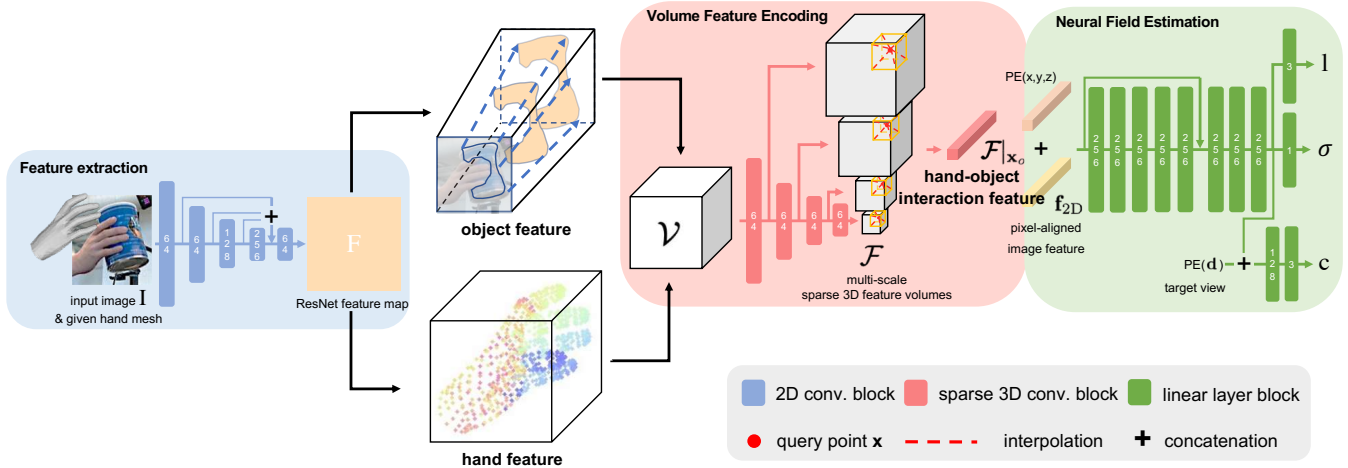


Fig. 3: HandNeRF takes a single RGB image and predicts the volume density, color radiance, and semantic label of each query point in a neural field. It explicitly encodes the correlation between hand and object features in 3D space, which provides more accurate 3D reconstruction and novel view synthesis.

feature extraction, sparse 3D convolution layers [7], [4] for volume feature encoding, and linear layers for the neural field estimation. During training, the estimated semantic neural radiance field is validated by projecting on sparse views. HandNeRF extracts the 3D hand feature \mathbf{f}_h and the 2D object feature \mathbf{f}_o utilizing a 3D hand mesh and 2D object segmentation and explicitly encode the interaction feature.

Input Features. We deproject a 2D image feature extracted from an image to the point in the 3D volume, for the 3D hand feature \mathbf{f}_h and the 2D object feature \mathbf{f}_o in Equation (4). The 3D hand feature is made of three components: $\mathbf{f}_h = [\mathbf{h}^\top \ \phi(\bar{\mathbf{m}}_i)^\top \ \psi(i)^\top]^\top$. \mathbf{h} encodes the visual context of hand-object interaction that is obtained from the 2D image feature at the projection of the centroid of the i^{th} face, $\bar{\mathbf{m}}_i$ in the 3D hand mesh. $\phi(\bar{\mathbf{m}}_i)$ is a positional encoding of the centroid, and $\psi(i)$ is the positional encoding of the face index. $\psi(i)$ semantically differentiates a 3D hand point \mathbf{x}_h from different points that are empty or belong to different hand faces and an object. The 2D object features is designed in a similar fashion: $\mathbf{f}_o = [\mathbf{o}^\top \ \phi(\mathbf{x}_o)^\top \ \mathbf{0}^\top]^\top$, where \mathbf{o} is the 2D image feature at the projection of \mathbf{x}_o .

3D CNN Design. We correlate the 3D hand feature \mathbf{f}_h and the 2D object feature \mathbf{f}_o with a sparse 3D CNN [7], [4] that takes the feature volume \mathcal{V} as input, to learn an interaction feature \mathcal{F} . \mathcal{V} rasterizes 3D points in the neural radiance field with a voxel size of $5\text{mm} \times 5\text{mm} \times 5\text{mm}$. Before the rasterization, 3D coordinates of object points are perturbed by a random Gaussian noise during training, for augmentation. The sparse 3D CNN consists of multiple sparse 3D convolutional layers and down-sampling layers. It produces multi-scale feature volumes, which conceptually add up to the interaction feature volume \mathcal{F} by concatenation along the feature channel dimension. In practice, we keep the multi-scale feature volumes separated and extract the interaction feature $\mathcal{F}|_{\mathbf{x}}$ of a query point \mathbf{x} per volume.

IV. EXPERIMENTS

In this section, we first validate our design choices for the method development by conducting detailed ablation studies. Then, we evaluate HandNeRF by comparing with state-of-the-art baselines [42], [41], [3] that are adapted to be trained on sparse view images without an object template and to be tested on a single image, both quantitatively and qualitatively. In particular, we adapted IHOI [41] to training without a template-based object annotation, instead using sparse view images, and named it as IHOINeRF. For IHOINeRF, training with semantic labels fails to converge where reconstruction accuracy for hand and object cannot be measured.

Metrics. We conduct the comparison based on two criteria: novel view rendering quality and the reconstruction accuracy of hand-object interactions. To assess the rendering quality, we use three metrics by comparing with the ground truth images: peak signal-to-noise ratio (PSNR), structural similarity index (SSIM), and LPIPS [43]. Note that only the foreground regions (hand and object) are considered for evaluation. For the 3D reconstruction accuracy, we compare 3D distance with the ground truth by converting the reconstructed neural radiance field to a 3D mesh using Marching cubes algorithm [21]. We evaluate hand and object separately using 3D segmentation from the predicted semantics. Using the converted meshes, we measure 3D reconstruction error in the forms of F-scores with 5mm and 10mm thresholds, and Chamfer distance (CD) in millimeters.

Datasets. We use two datasets for comparison: DexYCB [2] and HO-3D v3 [10]. DexYCB and HO-3D v3 datasets consist of multiview RGB(D) sequences of hand-object interactions with annotation of MANO [32] hand mesh parameters, 6D object poses, and object segmentation. The MANO hand mesh and object segmentation are used as input to HandNeRF for training and testing. In DexYCB, a single hand performing hand-over of a single object is captured from 8

TABLE I: An ablation study on DexYCB dataset shows that our model (M5) provides the highest rendering quality and F-scores, and the lowest Chamfer Distance (mm) for the whole and object geometry of the novel hand-objct interaction scenes. The subscripts w , o , and h indicate the evaluation for the whole, object, and hand geometry, respectively.

Method	Architect.	PSNR \uparrow	SSIM \uparrow	LPIPS \downarrow	F $_w$ -5 \uparrow	F $_w$ -10 \uparrow	CD $_w$ \downarrow	F $_o$ -5 \uparrow	F $_o$ -10 \uparrow	CD $_o$ \downarrow	F $_h$ -5 \uparrow	F $_h$ -10 \uparrow	CD $_h$ \downarrow
M1: $\mathbf{f}_h, \mathbf{f}_o + \mathbf{f}_{2D}$	Transf.	19.40	0.63	0.30	0.36	0.64	0.85	0.32	0.56	1.57	0.27	0.55	1.42
M2: \mathbf{f}_{2D}	3D CNN	19.09	0.60	0.31	0.30	0.56	1.17	0.28	0.47	2.90	0.19	0.49	1.56
M3: $\mathbf{f}_h, \mathbf{f}_o$		20.11	0.65	0.27	0.47	0.78	0.30	0.41	0.68	0.62	0.54	0.92	0.12
M4: $\mathbf{f}_h + \mathbf{f}_{2D}$		20.31	0.68	0.26	0.40	0.68	0.79	0.30	0.53	1.73	0.54	0.92	0.09
M5 (ours): $\mathbf{f}_h, \mathbf{f}_o + \mathbf{f}_{2D}$		21.66	0.70	0.24	0.47	0.79	0.27	0.43	0.70	0.56	0.53	0.91	0.10

views, and 5 sequences per object are recorded where each sequence shows a distinct grasp pattern. Per object, we split the data to 4 sequences for training and 1 sequence for testing to validate generalization to novel hand grasps. In Ho-3D v3, a single object grasped by a single hand is captured from 5 views and 1 sequence per object is recorded where a grasping hand pose changes over time over the course of object manipulation. Per object, we split the data to training and testing sets that have significantly different grasping hand poses, for the validation of the generalization to novel grasps.

A. Ablation Study

We conduct the ablation study on DexYCB to measure the impact of our design choices summarized in Table I. To focus on evaluation of generalization to novel grasp configurations, which are novel interaction between the hand and object, we train each method per object and average the metrics in the table. We use 4 objects with distinct shapes: ‘Cracker Box’, ‘Banana’, ‘Power Drill’, and ‘Coffee Can’. In inference time, all methods use the same 3D hand mesh and 2D object segmentation provided in DexYCB. We validate the following three hypotheses.

H1: Is the learned hand-object interaction feature effective for regulating the scene reconstruction? Our main hypothesis is that hand-object interactions are highly structured, resulting in precise 3D reconstruction of the grasped object given the 3D hand shape. We compare two methods to validate this hypothesis: (M2: \mathbf{f}_{2D}) a method similar to PixelNeRF [42] that uses the 2D image feature without the 3D hand feature and (M3: $\mathbf{f}_h, \mathbf{f}_o$) a method that uses the 3D hand and 2D object feature without the 2D image feature. By exploiting the 3D hand feature, M3 successfully imposes constraints on the relative geometries of hand and object, and provides better generalization to novel hand-object interactions. Table I shows that M3 achieves nearly 1.5 to 2 times higher F-scores and a large reduction of CD compared to M2. The results support that our learned interaction feature \mathcal{F} that encodes hand-object interactions is effective to infer a 3D object geometry without its 3D ground truth. The performance of the 3D feature is more pronounced for our method (M4: $\mathbf{f}_h, \mathbf{f}_o + \mathbf{f}_{2D}$) that leverages both the 2D image feature and the 3D feature.

H2: Is the 2D object feature useful? HandNeRF differs from the existing approaches [41], [3] by using explicit representation of an object with respect to a 3D hand. To verify the effectiveness of the 2D object feature, we compare

two methods: (M4: $\mathbf{f}_h + \mathbf{f}_{2D}$) a method that implicitly learns the hand-object interactions similar to IHOI [41] and (M5: $\mathbf{f}_h, \mathbf{f}_o + \mathbf{f}_{2D}$) our method that explicitly models the interactions through the 2D object feature. As shown in Table I, M4 tends to overfit to hand reconstruction and produces poor results for object reconstruction. This implies that without the explicitly defined 2D object feature and its correlation with the hand pose, a strong prior coming from the given hand pose information dominates the prediction while ignoring object information from an input image.

H3: Is a 3D CNN robust to overfitting? Learning hand-object interaction from Equation (2) is challenging due to the requirement of a large number of data. Instead, we approximate the pairwise relationship using a 3D CNN in Equation (3). We validate our conjecture by comparing a method (M1) that can directly learn the relationship between hand and object using Transformer [38]. The Transformer-based method correlates every pair of the hand features \mathbf{f}_h and the object features \mathbf{f}_o by adding the weighted sum of the each other’s features to, where the weights are the attention scores calculated by cross-attention mechanism. With the transformer features, we build a feature volume \mathcal{V} with the correlated \mathbf{f}_h and \mathbf{f}_o , and subsample to get multi-scale feature volumes of an interaction feature \mathcal{F} .

As shown in Table I, using the 3D CNN (M5) outperforms the Transformer variant (M1) in all metrics, especially in 3D reconstruction of objects. The result indicates that our method based on a 3D CNN is resilient to overfitting, given a small number of training scenes per object (~ 200). For example, M1 converges to 26.08 PSNR during training on hand-object interaction scenes of Banana, while the testing time accuracy is 21.48 PSNR. On the contrary, while having similar training loss (26.03 PSNR), our 3D CNN-based HandNeRF achieves 22.45 PSNR at the testing time. Moreover, the model complexity of the Transformer variant is over 10 times than ours, comparing the number of model parameters (271.K vs. 2.1K).

B. Comparison with State-of-the-art Methods

Generalization to novel grasps. We first evaluate the generalization to novel grasps on the objects seen during training (without 3D CAD model). Each method is trained per object. The same objects in the ablation study are used for quantitative evaluation on DexYCB. For quantitative evaluation on HO3D v3, we use 3 objects with distinct shapes: ‘Bleach Cleanser’, ‘Potted Meat Can’, and ‘Scissors’.

TABLE II: We compare our method with state-of-the-art baselines on DexYCB [2] and HO-3D v3 [10]. The subscripts w , o , and h indicate the evaluation for the whole, object, and hand geometry, respectively. MPJPEs (mean per joint position error) of the mesh estimate are 12mm and 34mm in DexYCB and HO3D v3, respectively. † indicates use of ground truth 3D hand meshes for inputs, otherwise the hand mesh estimated from HandOccNet [26] is used.

Method	Dataset	PSNR↑	SSIM↑	LPIPS↓	F _w -5 ↑	F _w -10 ↑	CD _w ↓	F _o -5 ↑	F _o -10 ↑	CD _o ↓	F _h -5 ↑	F _h -10 ↑	CD _h ↓
PixelNeRF	DexYCB	19.09	0.60	0.31	0.30	0.56	1.17	0.28	0.47	2.90	0.19	0.49	1.56
IHOINeRF		18.49	0.60	0.31	0.31	0.60	1.15	—	—	—	—	—	—
IHOINeRF†		19.82	0.64	0.27	0.38	0.69	0.54	—	—	—	—	—	—
MonoNHR		19.36	0.64	0.30	0.37	0.62	3.19	0.25	0.43	8.59	0.49	0.89	0.11
MonoNHR†		19.66	0.66	0.29	0.40	0.64	3.05	0.26	0.45	8.58	0.55	0.92	0.08
HandNeRF		21.19	0.68	0.25	0.44	0.77	0.31	0.42	0.68	0.59	0.46	0.88	0.12
HandNeRF†		21.66	0.70	0.24	0.47	0.79	0.27	0.43	0.70	0.56	0.53	0.91	0.10
PixelNeRF	HO3D v3	18.82	0.65	0.23	0.38	0.69	0.75	0.36	0.58	1.14	0.29	0.68	0.41
IHOINeRF		18.55	0.65	0.23	0.28	0.56	1.15	—	—	—	—	—	—
IHOINeRF†		19.40	0.68	0.21	0.41	0.73	0.65	—	—	—	—	—	—
MonoNHR		16.98	0.60	0.21	0.28	0.53	2.09	0.19	0.37	3.49	0.33	0.65	0.64
MonoNHR†		19.34	0.70	0.22	0.45	0.74	0.97	0.36	0.59	1.50	0.52	0.92	0.08
HandNeRF		18.04	0.63	0.23	0.38	0.70	0.35	0.40	0.66	0.41	0.45	0.51	0.78
HandNeRF†		20.54	0.74	0.18	0.51	0.83	0.19	0.47	0.74	0.31	0.54	0.94	0.08

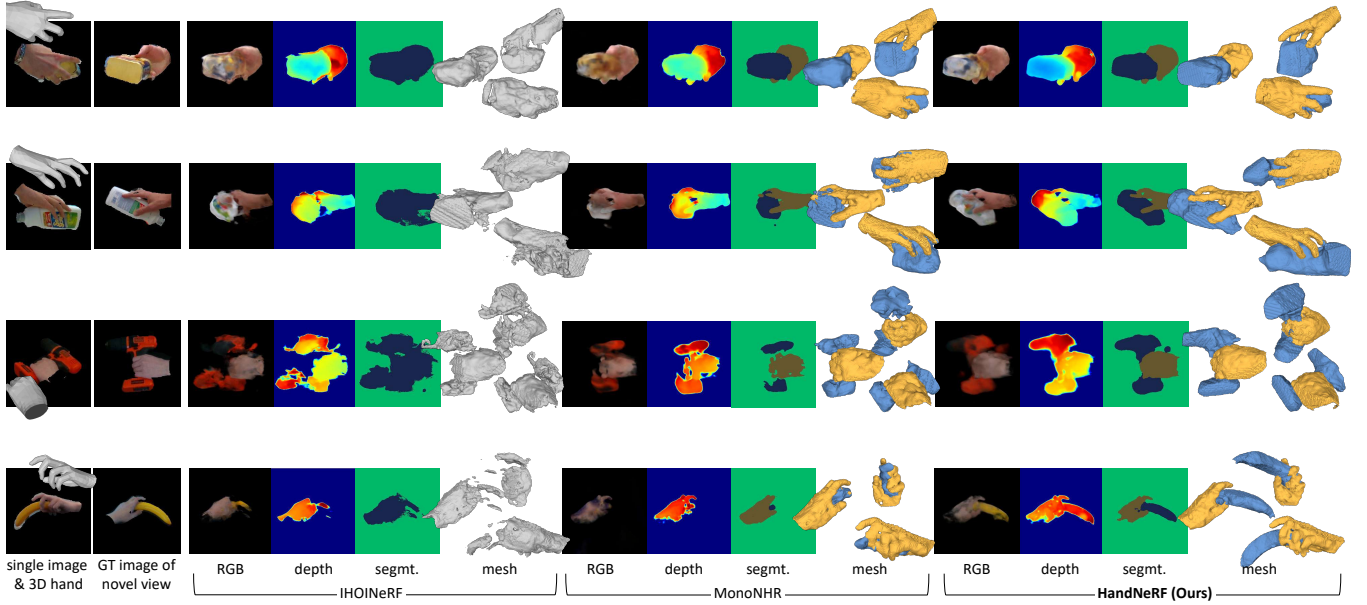


Fig. 4: Qualitative results of novel view synthesis (image, depth, and semantic segmentation) and 3D mesh on DexYCB [2] and HO3D v3 [9]. Ground truth hand meshes are used as input.

TABLE III: We evaluate HandNeRF by comparing it with state-of-the-art baselines on unseen objects of DexYCB [2]. The subscripts w , o , and h indicate the evaluation for the whole, object, and hand geometry, respectively. The mesh estimate inputs of IHOINeRF [41], MonoNHR [3], and HandNeRF are from HandOccNet [26] trained on DexYCB. † indicates using ground truth 3D hand meshes.

Method	PSNR↑	SSIM↑	LPIPS↓	F _w -5 ↑	F _w -10 ↑	CD _w ↓	F _o -5 ↑	F _o -10 ↑	CD _o ↓	F _h -5 ↑	F _h -10 ↑	CD _h ↓
PixelNeRF	18.85	0.58	0.34	0.21	0.47	1.09	0.22	0.44	1.31	0.10	0.31	2.09
IHOINeRF	18.05	0.56	0.36	0.11	0.24	625.30	—	—	—	—	—	—
IHOINeRF†	20.21	0.64	0.31	0.32	0.51	1.89	—	—	—	—	—	—
MonoNHR	17.04	0.52	0.37	0.26	0.51	1.52	0.17	0.34	2.89	0.37	0.73	0.73
MonoNHR†	19.06	0.63	0.31	0.48	0.71	1.13	0.43	0.64	1.76	0.53	0.82	0.49
HandNeRF	18.85	0.55	0.33	0.30	0.61	0.62	0.25	0.49	0.85	0.36	0.69	0.88
HandNeRF†	20.83	0.66	0.27	0.51	0.75	0.72	0.46	0.68	1.11	0.51	0.80	0.52

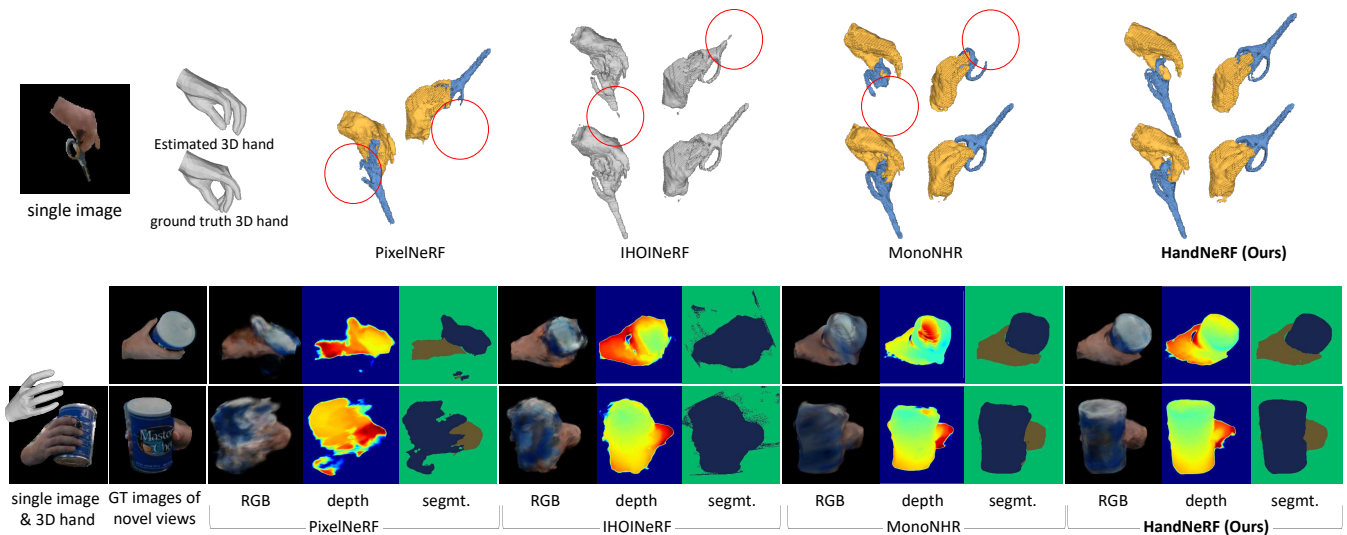


Fig. 5: Qualitative results of novel view synthesis (image, depth, and semantic segmentation) and 3D mesh on DexYCB [2] and HO3D v3 [9], when given hand mesh estimation of HandOccNet [26]. The bottom row results of IHOINeRF, MonoNHR, and HandNeRF for scissors are using ground truth 3D hand mesh for reference.

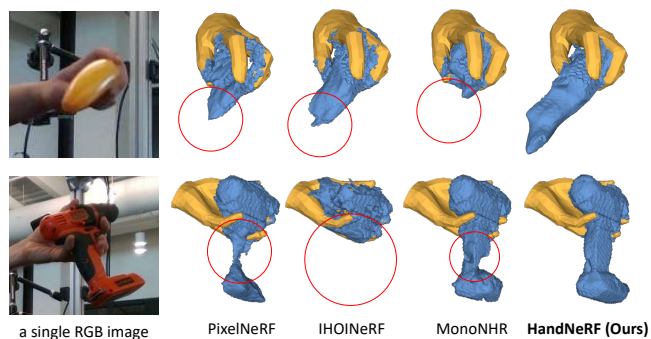


Fig. 6: Qualitative results of generalization to novel object shapes. The reconstructed 3D object mesh is visualized along with the ground truth MANO hand mesh, which is used as input. Despite the fact that ‘Banana’ and ‘Power Drill’ have significantly different shapes from those of the training data, HandNeRF achieves robust 3D reconstruction compared with the baselines.

Table II presents quantitative evaluation on DexYCB and HO3D v3. Given the ground truth grasping hand shape, HandNeRF shows the highest rendering quality scores and the highest F-scores, and the lowest CD (mm) for the whole and object geometry of the novel hand-object interaction scenes. For example, HandNeRF achieves approximately 1.5 times higher F-scores and significantly lower CD for object reconstruction than that of PixelNeRF [42] and MonoNHR [3]. The results prove that HandNeRF learns effective hand-object interaction priors compared with the baselines. Also, our model shows the strongest robustness to inaccuracies in the estimated hand mesh of HandOccNet. When the estimated hand meshes are used, IHOINeRF

and MonoNHR, which also take a 3D hand pose/shape as input, are overall outperformed by PixelNeRF. However, the proposed HandNeRF still shows significant accuracy margin against PixelNeRF, especially in 3D reconstruction of objects. We analyze that the explicit modeling of hand and object correlation using both the 3D hand feature and the 2D object feature is a key to the outperformance, which is also verified in the ablation study.

In Fig. 4 we further qualitatively evaluate HandNeRF by visually comparing novel view synthesis and 3D mesh with IHOINeRF and MonoNHR that also use 3D hand as input. Ground truth hand meshes are used as input. While the baselines can render the coarse texture of an object from a novel view, the 3D reconstruction of an object is very noisy and misaligned, and results in spatially inaccurate RGB and depth rendering. For example, IHOINeRF and MonoNHR only partially reconstruct the ‘Bleach Cleanser’ and render misaligned RGB images, as shown in the second row. In contrast, our HandNeRF infers more accurate 3D object geometry and renders spatially well-aligned images from novel views. We also demonstrate HandNeRF’s robustness to erroneous input hand meshes in Fig. 5, which is quantitatively verified in Table II. When the hand mesh estimation of HandOccNet [26] is used instead of the ground truth, a small pose error in the input hand mesh affects the outputs of IHOINeRF and MonoNHR significantly. These methods fail to recover half part of the scissors as shown at top, which implies the limitation of implicit interaction encoding. PixelNeRF renders poor RGB, depth, and segmentation from novel views for invisible surfaces due to high ambiguity of a single image as shown at the bottom of Fig. 5. On the contrary, HandNeRF retains the reasonable reconstruction quality when given inaccurate 3D hand input and renders

TABLE IV: We demonstrate the effectiveness of reconstruction of HandNeRF for a downstream task: grasping for robotic hand-over. We evaluate grasp quality of Contact-GraspNet [36]’s proposals on reconstruction of HandNeRF and the baselines. The hand-object interaction scenes of DexYCB [2] are used. † indicates using ground truth 3D hand meshes for the methods’ input.

Input	Method	Grasp proposal success ratio \uparrow
RGB	PixelNeRF	0.46
	IHOINeRF	0.42
	IHOINeRF†	0.44
	MonoNHR	0.36
	MonoNHR†	0.41
	HandNeRF	0.63
	HandNeRF†	0.65
RGBD	-	0.26
GT mesh	-	0.77

more accurate images from novel views highly different from an input view.

Generalization to novel object shape. We evaluate the generalization to novel hand grasps on novel objects on DexYCB. We train each method on 15 DexYCB objects and test on unseen 4 DexYCB objects, which are namely, ‘Sugar Box’, ‘Mustard Bottle’, ‘Power Drill’, and ‘Banana’.

As shown in Table III and Fig. 6, HandNeRF consistently outperforms the baselines in most of the metrics. Especially, HandNeRF reconstructs robust object meshes despite substantial dissimilarity between the shapes of objects in the training and testing sets. Due to depth ambiguity of a 2D single RGB image, PixelNeRF fails to recover the overall shape of the object. For example, ‘Banana’ is only partially reconstructed, as its length is unclear in the input. IHOINeRF is highly sensitive to noise in hand input as shown in the second and third rows of Table III, over 2 times drop in F-scores. MonoNHR is prone to overfitting to hand reconstruction and show the lowest novel view synthesis metrics when the estimated hand meshes are used. The results demonstrate HandNeRF’s better generalization capability, and we conjecture that the explicit encoding of the hand and object geometry effectively regularizes the possible geometry of the novel object.

Downstream task. Among various applications of the reconstruction of hand-object interaction scenes, we demonstrate its usefulness in grasping for robotic hand-over. We run the state-of-the-art grasp proposal network, Contact-GraspNet [36] on reconstructed meshes of HandNeRF, the baselines [42], [41], [3], pointclouds obtained from RGBD images, and the ground truth object mesh for reference. We filter out the grasps that collide with the hand. We measure the ratio of successful grasp proposals, where a grasp is counted successful if it envelops at least some part of the ground truth object geometry without colliding with it. Multiple reconstruction results of two DexYCB objects, namely, ‘Banana’ and ‘Power Drill’ from Table II are used for the evaluation since Contact-GraspNet performs well on

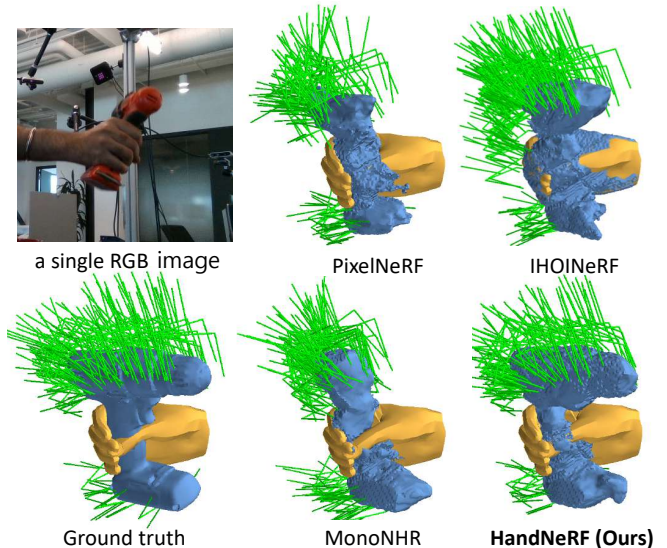


Fig. 7: Qualitative results of Contact-GraspNet [36]’s grasp proposals on reconstructed meshes of HandNeRF and the baselines. The ground truth MANO hand mesh, which is used as input and grasp collision avoidance, is also visualized. For reference, we provide the proposals on the ground truth.

the ground truth object meshes of these objects.

HandNeRF’s object reconstruction enables a 1.5 times higher grasp proposal success ratio compared to baselines, as shown in Table IV. Without depth information, HandNeRF achieves a 63% grasp success ratio, approaching the 77% achieved by Contact-GraspNet using ground truth meshes and far exceeding the 26% from RGBD point clouds. Fig. 7 visually demonstrates how HandNeRF’s more accurate reconstruction increases successful grasp proposals. Although the surface is locally coarse, HandNeRF’s reconstructed surface geometry is far more reasonable globally than baselines, and enables more accurate execution of the grasping downstream task.

V. LIMITATION AND FUTURE WORK

The limitation of our method in practice is that it strongly depends on hand mesh estimation of off-the-shelf methods. Despite the advance of the recent methods [33], [26], [23], when the hand is severely occluded by the object, the estimated mesh is not accurate enough for inferring further correlation between the hand and object geometry. In such cases, the wrongly estimated hand information can rather hurt the object reconstruction. In the future, we will explore to integrate the hand mesh estimation into our system along with the uncertainty modeling to adjust the hand mesh’s impact to the final output.

Despite outperformance, our synthesized RGB images are still blurry, when rendered from significantly different view from an input view. Inspired by recent progress on 3D scene generation via language grounding [29], another avenue for future research will be to leverage self-supervised perceptual

supervision, such as CLIP [30] feature consistency and object coherency.

VI. CONCLUSION

This work investigates representation learning for hand-object interactions from a single RGB image. We propose HandNeRF, a method that predicts the semantic neural radiance field of the interaction scenes. The key novelty is the utilization of hand shape to constrain the relative 3D configuration of hands and objects, encoding their correlation explicitly. Unlike existing works, HandNeRF does not require object templates for training and testing, avoiding expensive 3D labeling. Instead, it is supervised with sparse view RGB images, where conventional multi-view reconstruction methods, such as SfM (Structure from Motion), do not apply. HandNeRF outperforms state-of-the-art baselines in rendering and reconstruction on real-world data. Further, we demonstrate improved performance on downstream tasks resulting from HandNeRF’s more accurate object meshes, both quantitatively and qualitatively.

REFERENCES

- [1] Z. Cao, I. Radosavovic, A. Kanazawa, and J. Malik, “Reconstructing hand-object interactions in the wild,” in *ICCV*, 2021.
- [2] Y.-W. Chao, W. Yang, Y. Xiang, P. Molchanov, A. Handa, J. Tremblay, Y. S. Narang, K. Van Wyk, U. Iqbal, S. Birchfield, *et al.*, “Dexycb: A benchmark for capturing hand grasping of objects,” in *CVPR*, 2021.
- [3] H. Choi, G. Moon, M. Armando, V. Leroy, K. M. Lee, and G. Rogez, “Mononhr: Monocular neural human renderer,” in *3DV*, 2022.
- [4] S. Contributors, “Sponcv: Spatially sparse convolution library,” <https://github.com/traveller59/sponcv>, 2022.
- [5] B. Doosti, S. Naha, M. Mirbagheri, and D. J. Crandall, “Hope-net: A graph-based model for hand-object pose estimation,” in *CVPR*, 2020.
- [6] L. Ge, Z. Ren, Y. Li, Z. Xue, Y. Wang, J. Cai, and J. Yuan, “3d hand shape and pose estimation from a single rgb image,” in *CVPR*, 2019.
- [7] B. Graham, M. Engelcke, and L. van der Maaten, “3d semantic segmentation with submanifold sparse convolutional networks,” in *CVPR*, 2018.
- [8] T. Groueix, M. Fisher, V. G. Kim, B. Russell, and M. Aubry, “AtlasNet: A Papier-Mâché Approach to Learning 3D Surface Generation,” in *CVPR*, 2018.
- [9] S. Hampali, M. Rad, M. Oberweger, and V. Lepetit, “Honnotate: A method for 3d annotation of hand and object poses,” in *CVPR*, 2020.
- [10] S. Hampali, S. D. Sarkar, and V. Lepetit, “Ho-3d.v3: Improving the accuracy of hand-object annotations of the ho-3d dataset,” *arXiv*, 2021.
- [11] S. Hampali, S. D. Sarkar, M. Rad, and V. Lepetit, “Keypoint transformer: Solving joint identification in challenging hands and object interactions for accurate 3d pose estimation,” in *CVPR*, 2022.
- [12] Y. Hasson, B. Tekin, F. Bogo, I. Laptev, M. Pollefeys, and C. Schmid, “Leveraging photometric consistency over time for sparsely supervised hand-object reconstruction,” in *CVPR*, 2020.
- [13] Y. Hasson, G. Varol, D. Tzionas, I. Kalevtykh, M. J. Black, I. Laptev, and C. Schmid, “Learning joint reconstruction of hands and manipulated objects,” in *CVPR*, 2019.
- [14] K. He, X. Zhang, S. Ren, and J. Sun, “Deep residual learning for image recognition,” in *CVPR*, 2016.
- [15] A. Jain, M. Tancik, and P. Abbeel, “Putting nerf on a diet: Semantically consistent few-shot view synthesis,” in *ICCV*, 2021.
- [16] K. Karunratanakul, J. Yang, Y. Zhang, M. J. Black, K. Muandet, and S. Tang, “Grasping field: Learning implicit representations for human grasps,” in *3DV*, 2020.
- [17] Y. Kwon, D. Kim, D. Ceylan, and H. Fuchs, “Neural Human Performer: Learning generalizable radiance fields for human performance rendering,” in *NeurIPS*, 2021.
- [18] V. Leroy, J. Franco, and E. Boyer, “Volume sweeping: Learning photoconsistency for multi-view shape reconstruction,” *IJCV*, 2021.
- [19] S. Liu, H. Jiang, J. Xu, S. Liu, and X. Wang, “Semi-supervised 3d hand-object poses estimation with interactions in time,” in *CVPR*, 2021.
- [20] M. Loper, N. Mahmood, J. Romero, G. Pons-Moll, and M. J. Black, “Smpl: A skinned multi-person linear model,” *ACM TOG*, 2015.
- [21] W. E. Lorensen and H. E. Cline, “Marching cubes: A high resolution 3d surface construction algorithm,” *SIGGRAPH*, 1987.
- [22] B. Mildenhall, P. P. Srinivasan, M. Tancik, J. T. Barron, R. Ramamoorthi, and R. Ng, “Nerf: Representing scenes as neural radiance fields for view synthesis,” in *ECCV*, 2020.
- [23] G. Moon, H. Choi, and K. M. Lee, “Accurate 3d hand pose estimation for whole-body 3d human mesh estimation,” in *CVPR workshop*, 2022.
- [24] G. Moon, S.-I. Yu, H. Wen, T. Shiratori, and K. M. Lee, “Interhand2.6m: A dataset and baseline for 3d interacting hand pose estimation from a single rgb image,” in *ECCV*, 2020.
- [25] M. Niemeyer, J. T. Barron, B. Mildenhall, M. S. Sajjadi, A. Geiger, and N. Radwan, “Regnerf: Regularizing neural radiance fields for view synthesis from sparse inputs,” in *CVPR*, 2022.
- [26] J. Park, Y. Oh, G. Moon, H. Choi, and K. M. Lee, “Handocnet: Occlusion-robust 3d hand mesh estimation network,” in *CVPR*, 2022.
- [27] G. Pavlakos, V. Choutas, N. Ghorbani, T. Bolkart, A. A. Osman, D. Tzionas, and M. J. Black, “Expressive body capture: 3d hands, face, and body from a single image,” in *CVPR*, 2019.
- [28] S. Peng, Y. Zhang, Y. Xu, Q. Wang, Q. Shuai, H. Bao, and X. Zhou, “Neural body: Implicit neural representations with structured latent codes for novel view synthesis of dynamic humans,” in *CVPR*, 2021.
- [29] B. Poole, A. Jain, J. T. Barron, and B. Mildenhall, “Dreamfusion: Text-to-3d using 2d diffusion,” *arXiv*, 2022.
- [30] A. Radford, J. W. Kim, C. Hallacy, A. Ramesh, G. Goh, S. Agarwal, G. Sastry, A. Askell, P. Mishkin, J. Clark, *et al.*, “Learning transferable visual models from natural language supervision,” in *ICML*, 2021.
- [31] G. Rogez, J. S. Supancic, and D. Ramanan, “Understanding everyday hands in action from rgb-d images,” in *ICCV*, 2015.
- [32] J. Romero, D. Tzionas, and M. J. Black, “Embodied hands: Modeling and capturing hands and bodies together,” in *SIGGRAPH Asia*, 2017.
- [33] Y. Rong, T. Shiratori, and H. Joo, “Frankmocap: A monocular 3d whole-body pose estimation system via regression and integration,” in *ICCV Workshops*, 2021.
- [34] S. Saito, Z. Huang, R. Natsume, S. Morishima, A. Kanazawa, and H. Li, “Pifu: Pixel-aligned implicit function for high-resolution clothed human digitization,” in *ICCV*, 2019.
- [35] S. Sridhar, F. Mueller, M. Zollhöfer, D. Casas, A. Oulasvirta, and C. Theobalt, “Real-time joint tracking of a hand manipulating an object from rgb-d input,” in *ECCV*, 2016.
- [36] M. Sundermeyer, A. Mousavian, R. Triebel, and D. Fox, “Contact-graspnet: Efficient 6-dof grasp generation in cluttered scenes,” in *ICRA*, 2021.
- [37] B. Tekin, F. Bogo, and M. Pollefeys, “H+ o: Unified egocentric recognition of 3d hand-object poses and interactions,” in *CVPR*, 2019.
- [38] A. Vaswani, N. Shazeer, N. Parmar, J. Uszkoreit, L. Jones, A. N. Gomez, Ł. Kaiser, and I. Polosukhin, “Attention is all you need,” in *NeurIPS*, 2017.
- [39] Q. Wang, Z. Wang, K. Genova, P. P. Srinivasan, H. Zhou, J. T. Barron, R. Martin-Brualla, N. Snavely, and T. Funkhouser, “Ibrnet: Learning multi-view image-based rendering,” in *CVPR*, 2021.
- [40] H. Xu, T. Alldieck, and C. Sminchisescu, “H-nerf: Neural radiance fields for rendering and temporal reconstruction of humans in motion,” in *NeurIPS*, 2021.
- [41] Y. Ye, A. Gupta, and S. Tulsiani, “What’s in your hands? 3d reconstruction of generic objects in hands,” in *CVPR*, 2022.
- [42] A. Yu, V. Ye, M. Tancik, and A. Kanazawa, “pixelnerf: Neural radiance fields from one or few images,” in *CVPR*, 2021.
- [43] R. Zhang, P. Isola, A. A. Efros, E. Shechtman, and O. Wang, “The unreasonable effectiveness of deep features as a perceptual metric,” in *CVPR*, 2018.
- [44] S. Zhi, T. Laidlow, S. Leutenegger, and A. J. Davison, “In-place scene labelling and understanding with implicit scene representation,” in *ICCV*, 2021.
- [45] C. Zimmermann, M. Argus, and T. Brox, “Contrastive representation learning for hand shape estimation,” in *GCPD*, 2022.
- [46] C. Zimmermann, D. Ceylan, J. Yang, B. Russell, M. Argus, and T. Brox, “Freihand: A dataset for markerless capture of hand pose and shape from single rgb images,” in *CVPR*, 2019.